INSTITUTE OF PHYSICS PUBLISHING JOURNAL OF PHYSICS: CONDENSED MATTER

J. Phys.: Condens. Matter **14** (2002) 2799–2823 PII: S0953-8984(02)28153-9

Conceptual improvements of the KKR method

N Papanikolaou[1], **R Zeller**[2] **and P H Dederichs**[2]

[1] Martin Luther Universität, Halle-Wittenberg, Fachbereich Physik, Fachgruppe Theoretische Physik, D-06099 Halle, Germany
[2] Institut für Festkörperforschung, Forschungszentrum Jülich, D-52425 Jülich, Germany

Received 23 August 2001, in final form 18 September 2001
Published 8 March 2002
Online at stacks.iop.org/JPhysCM/14/2799

Abstract

We review some recent conceptual improvements of the Korringa–Kohn–Rostoker (KKR) Green function method for electronic structure calculations. After an introduction into the KKR–Green function method we present an extension of this method into an accurate full-potential scheme, which allows calculation of forces and lattice relaxations. The additional numerical effort compared to the atomic sphere approximation scales only linear with the number of atoms. In addition, we discuss the recently developed screened KKR method which represents a reformulation of the multiple scattering theory with exponentially decreasing structure constants. This method, which has the same accuracy as the standard KKR method, exhibits strong advantages for two-dimensional systems like multilayers or surfaces, since the numerical effort scales linearly with the number of layers. The strength of both methods is illustrated in typical applications.

1. The KKR method

1.1. Introduction

The KKR method of band structure calculations was already introduced in 1947 by Korringa [1] and in 1954 by Kohn and Rostoker [2]. A characteristic feature of this method is the use of the multiple scattering theory for solving the Schrödinger equation. In this way the problem is broken up into two parts. First, one solves the *single scattering problem* presented by a single potential in free space. Second, one solves the *multiple scattering problem* by demanding that the incident wave to each potential should be the sum of the outgoing waves from all other scattering centres. The resulting equations show a beautiful separation between potential and structural properties being characteristic for the KKR method. Another characteristic feature of the KKR method is that it does not rely on a finite basis set for the expansion of the wave functions as practically all other methods of electronic structure calculations do. The choice of the basis functions usually completely characterizes each method and is the decisive factor for the successes and limitations of the method. In the KKR method one solves the radial

Schrödinger equation for each site exactly, which in a sense may be interpreted as using a size-, angular momenta- and energy-adapted basis set, which is optimally small.

While the traditional KKR band structure scheme was not very popular, the method experienced a revival as a Green function method. Here the full strength of multiple scattering theory, being at the heart of the KKR method, can be much better exploited than in the wave function scheme. In particular, due to the introduction of the complex energy integration it is well suited for ground-state calculations, with an efficiency comparable to typical diagonalization methods. This development opened the way to deal with solids with reduced symmetry, as, for example an impurity in an otherwise ordered host crystal, or surfaces, layered systems, etc. Another important application is the investigation of randomly disordered alloys by means of the coherent potential approximation (KKR-CPA). It is basically the availability of the Green function which makes this method so powerful and which uniquely distinguishes it from other electronic structure methods.

The original KKR method and also the Green function version for impurities are well known and treated in several books [3–6]. For a special summary of multiple scattering methods related to KKR we refer to the proceedings of an MRS Symposium [7]. Here we want to review recent advances in conceptual improvements of the KKR–Green function method, which have been mostly achieved in our group. In section 2 we present the extension of the KKR method to 'full' potentials and show that this method allows calculation of forces and lattice relaxations. The full potential method is very accurate and requires only a modest increase in computing time, since the additional effort scales linearly with the number of atoms. The calculated lattice relaxations around defects in metals and semiconductors are compared with EXAFS data and results obtained by other *ab initio* methods.

In section 3 we present the screened or tight binding KKR method recently introduced in collaboration with the Vienna/Budapest group [8]. This is a new and exact reformulation of multiple scattering with structure constants which decay exponentially in real space and which can therefore be cut off after several shells. We demonstrate that this screened KKR method has the same accuracy as the usual KKR method. For three-dimensional systems it eliminates the difficulties in calculating the KKR structure constants. However the greatest advantage occurs for systems with two-dimensional translational symmetry like multilayers and surfaces, since here the numerical effort shows N-scaling behaviour. The strength of the method is demonstrated in typical applications. Section 4 summarizes the main result and gives an outlook for future research.

1.2. Green function and charge density

The strategy of Green function calculations consists of avoiding the calculation of eigenvalues E_α and eigenstates ψ_α of the Hamiltonian, but rather calculating directly the Green function $G(\boldsymbol{r}, \boldsymbol{r}'; E)$ of the system, which is determined by the solution of the Schrödinger equation with a source term:

$$\big(-\partial_{\boldsymbol{r}}^2 + V(\boldsymbol{r}) - E\big)G(\boldsymbol{r}, \boldsymbol{r}'; E) = -\delta(\boldsymbol{r} - \boldsymbol{r}') \tag{1}$$

with atomic units $\hbar^2/2m = 1$ used here and in the following. Using the spectral representation for the (retarded) Green function

$$G(\boldsymbol{r}, \boldsymbol{r}'; E + \mathrm{i}\epsilon) = \sum_\alpha \frac{\psi_\alpha(\boldsymbol{r})\psi_\alpha^*(\boldsymbol{r}')}{E + \mathrm{i}\epsilon - E_\alpha} \tag{2}$$

it is easy to show that the charge density $n(\boldsymbol{r})$ can be directly expressed by an energy integral over the imaginary part of the Green function:

$$n(\boldsymbol{r}) \;=\; 2 \sum_{\substack{\alpha \\ E_\alpha < E_F}} |\psi_\alpha(\boldsymbol{r})|^2 = -\frac{2}{\pi} \int^{E_F} \mathrm{d}E \; \mathrm{Im}\, G(\boldsymbol{r}, \boldsymbol{r}; E). \tag{3}$$

This relation directly allows calculation of the charge density from the imaginary part of the Green function, which can be interpreted as the local density of states at the position $\boldsymbol{r}$. In this way the evaluation of the wave functions $\psi_\alpha(\boldsymbol{r})$ can be avoided. Due to the strong energy-dependent structure of the density of states, the evaluation of the energy integral is usually very cumbersome and typically about 10^3 energy points are needed in an accurate evaluation of this integral.

The numerical effort can be strongly decreased, if the analytical properties of the Green function $G(z)$ for complex energies $z = E + \mathrm{i}\Gamma$ are used. Since $G(z)$ is analytical in the whole complex energy plane, the energy integral can be transformed into a contour integral in the complex energy plane [9]

$$n(\boldsymbol{r}) = -\frac{2}{\pi} \mathrm{Im} \int_{E_B}^{E_F} \mathrm{d}z \, G(\boldsymbol{r}, \boldsymbol{r}; z) \tag{4}$$

where the contour starts at an energy E_B below the bottom of the valence bands, goes into the complex plane and comes back to the real axis at the Fermi level. Since for complex energies all structures of the Green function are broadened by the imaginary part Γ, the contour integral can be accurately evaluated by rather few energy points, typically 20–30, leading to a large saving of computer time. In this way Green function methods are competitive with diagonalization methods. Additional advantages occur for systems with two- or three-dimensional symmetry, since as a result of the energy broadening the $\boldsymbol{k}$-integration over the Brillouin zone requires for complex energies fewer $\boldsymbol{k}$-points. In the evaluation of the contour integral, special care is necessary for the piece of the path close to E_F, since here the full structure of $G(E)$ on the real axis reappears. Therefore the energy mesh should become increasingly denser when approaching E_F.

The integration over a complex energy contour can also be extended to finite temperatures by using the analytical properties of the Fermi–Dirac distribution [10]. Here the essential point is that the contour close to E_F is replaced by a sum over Matsubara energies $z_j = E_F + \mathrm{i}\pi(2j-1)kT$, $j = 1, 2, \ldots$. Then only complex energies are needed, since the energy point closest to E_F still has an imaginary part of πkT. This is of particular advantage for layered systems, where the two-dimensional Brillouin zone integration has to be evaluated by the special points method. Here the finite imaginary part πkT means an energy smearing of the $\boldsymbol{k}_\parallel$-dependent Green function $G(\boldsymbol{k}_\parallel; E)$, so that the $\boldsymbol{k}_\parallel$-dependence becomes smooth, ensuring a convergence of the $\boldsymbol{k}_\parallel$-integration.

It is worthwhile to remember that in density functional theory the eigenvalues and wave functions do not have a direct physical meaning, but are only auxiliary quantities introduced to evaluate the charge density. Using the shortcut of the complex energy integration is just in the spirit of density functional theory, and in this sense the method is similar to the density matrix method [11].

1.3. Green function and Dyson equation

The only effective way to determine the Green function $G(E)$ of a considered system is to relate it to a reference system, the Green function $G^0(E)$ of which is known. Let $H^0 + V$ be

the Hamiltonian of the real system considered, H^0 the one of the reference system, then the two Green functions are connected by the Dyson equation

$$G(E) \;=\; G^0(E) + G^0(E)\; V\; G(E) = [1 - G^0(E)V]^{-1} G^0(E) \tag{5}$$

which has to be solved to obtain $G(E)$.

The easiest reference system is the free space, since the Green function is known analytically. This can, e.g., be used to calculate the Green function of a cluster, or by exploiting the periodicity by means of Fourier transform, the Green function of an ideal crystal. This Green function can again be used to calculate the Green function for a point defect in an otherwise ideal crystal or of a clean surface. The latter may serve as the reference Green function, for example for an adatom on the surface. More details will be presented in section 1.5.

One important advantage of the Green function method is that one does not need an 'Ersatz geometry'. For instance, once the Green function of the ideal crystal is available, one can treat the problem of a single point defect exactly, i.e. without approximating it by a small cluster with a defect in the centre or by a periodically repeated supercell. Analogously, one can handle the problem of a single defect on a surface, once the Green function of the surface is available. The screened KKR method to be presented in section 3 even allows the treatment of arbitrary layered systems, such as e.g. a semi-infinite system like a surface or two coupled semi-infinite halfspaces.

1.4. Multiple scattering and the KKR–Green function

The Green function method within the frame of conventional KKR band structure method was proposed by Dupree [12], Beeby [13] and Morgan [14] and first applied in self-consistent calculations for impurities in metals by our group [15]. In this method one divides the whole space into non-overlapping and space-filling cells centred at position $\boldsymbol{R}^n$. In each cell the electrons are scattered by potentials v^n, which in this section are assumed to be spherically symmetric and centred at $\boldsymbol{R}^n$. By introducing cell-centred coordinates the Green function $G(\boldsymbol{r} + \boldsymbol{R}^n, \boldsymbol{r}' + \boldsymbol{R}^{n'}; E)$ can then be expanded in each cell as a function of $\boldsymbol{r}$ and $\boldsymbol{r}'$ into spherical harmonics:

$$\begin{aligned} G(\boldsymbol{r} + \boldsymbol{R}^n, \boldsymbol{r}' + \boldsymbol{R}^{n'}; E) = \delta_{nn'}\sqrt{E} \sum_L H_L^n(\boldsymbol{r}_\rangle; E) R_L^n(\boldsymbol{r}_\langle; E) \\ + \sum_{LL'} R_L^n(\boldsymbol{r}; E)\; G_{LL'}^{nn'}(E)\; R_{L'}^{n'}(\boldsymbol{r}'; E). \end{aligned} \tag{6}$$

Here $\boldsymbol{r}$ and $\boldsymbol{r}'$ are restricted to the cells n and n' and $\boldsymbol{r}_\langle$ and $\boldsymbol{r}_\rangle$ denote one of the two vectors $\boldsymbol{r}$ and $\boldsymbol{r}'$ which has the smaller or larger absolute value. The $R_L^n(\boldsymbol{r}; E)$ and $H_L^n(\boldsymbol{r}; E)$ are products of spherical harmonics and radial eigenfunctions to the central potential $v^n(r)$:

$$R_L^n(\boldsymbol{r}; E) = R_l^n(r; E)\, Y_L(\boldsymbol{r}) \tag{7}$$

$$H_L^n(\boldsymbol{r}; E) = H_l^n(r; E)\, Y_L(\boldsymbol{r}). \tag{8}$$

Here $R_L^n(\boldsymbol{r}, E)$ is the regular solution which varies at the origin as r^l and which represents the solution for an incoming spherical Bessel function $j_l(\sqrt{E}r)Y_L(\boldsymbol{r})$, while H_l^n is the corresponding irregular solution which varies as $1/r^{l+1}$ at the origin and is identical to the spherical Hankel function $h_l(\sqrt{E}r)$ outside the range of the potential. Both radial functions are connected by the Wronskian relation, which guarantees that the first term in equation (6) represents the exact Green function for the single potential $v^n(r)$ in free space. Since this term already satisfies the source condition $-\delta(\boldsymbol{r} - \boldsymbol{r}')$ for the Green function of equation (1), the

second term is source-free and contains in the double angular momentum expansion only the regular solutions R^n_L and $R^{n'}_{L'}$.

By construction, the expression (6) for the Green function satisfies in each cell n the general solution of the Schrödinger equation (1) for the Green function, while the matrix $G^{nn'}_{LL'}(E)$, the so-called *structural Green function*, describes the connection of the solutions in the different cells and thus contains all the information about the multiple scattering problem, which is in this way reduced to the solution of an algebraic problem. The clear separation between the single-site properties, described by the radial solutions $R^n_L(\boldsymbol{r})$ and $H^n_L(\boldsymbol{r})$ and the multiple scattering properties as described by the matrix $G^{nn'}_{LL'}$, is the main advantage of the KKR method.

In principle, the structural Green function matrix $G^{nn'}_{LL'}(E)$ can be determined by matching the solutions of the neighbouring cells at the cell boundaries. However at the cell boundaries the angular momentum expansion converges rather slowly, so that presumably a large $l_{\max}$ cut-off would be needed. The more elegant and at the same time more efficient way consists in using the power of multiple scattering theory, where the Green function is basically only needed in the inner region of the cell, where the potential is strong, so that the l-convergence does not represent a problem. As shown by Beeby [13] and others [4, 6, 12, 14], the structural Green function matrix can be determined from the corresponding matrix g in free space by the Dyson equation

$$G^{nn'}_{LL'}(E) = g^{nn'}_{LL'}(E) + \sum_{n''L''} g^{nn''}_{LL''}\, t^{n''}_{l''}\, G^{n''n'}_{L''L'} \tag{9}$$

where the t-matrix t^n_l for the potential $v^n(r)$ is given by

$$t^n_l(E) = \int_0^R \mathrm{d}r\; r^2\; j_l(\sqrt{E}r)\; v^n(r)\; R^n_l(r;\, E). \tag{10}$$

The derivation of this equation is lengthy and straightforward so that we refer for this to the literature cited above. An elementary derivation, also valid for the full-potential case, has been given by Zeller [19].

1.5. Crystals, impurities, surfaces, layers

In this section we discuss the solution of the Dyson equation for different geometries, representing the most important and time-consuming problem in the application of Green function methods. The most trivial case is a finite cluster of scattering centres in free space, where equation (9) has to be solved by direct inversion in real space. Naturally the computational effort might be reduced by exploiting the point symmetry of the cluster by means of group theory. The case of an ideal crystal is already a non-trivial example, where one can take advantage of the translation symmetry by means of the Fourier transform. For instance, for a crystal with one atom per unit cell, the t-matrix t_l is the same for all atoms, and the matrix $G^{nn'}_{LL'}$ depends only on the difference vector $\boldsymbol{R}^n - \boldsymbol{R}^{n'}$, as the free Green function $g^{nn'}_{LL'}$ always does. The Fourier-transformed Green function $\boldsymbol{G}(\boldsymbol{k}, E)$ is then given by

$$\mathbf{G}(\boldsymbol{k}, E) = [\mathbf{1} - \mathbf{g}(\boldsymbol{k}, E)\mathbf{t}(E)]^{-1}\mathbf{g}(\boldsymbol{k}, E) \tag{11}$$

where both $\mathbf{G}$ and $\mathbf{g}$ are matrices in angular momentum space. The Green function $G^{nn'}_{LL'}(E)$ in real space follows directly by backtransformation. The generalization to crystals with many atoms per unit cell is straightforward.

Let us now consider an impurity, or in general a localized region of perturbed potentials in an otherwise ideal crystal. By taking the ideal crystal Green function $G^{0,nn'}_{LL'}(E)$ as the

reference, the t-matrices $t_l^n = t_l^0 + \Delta t_l^n$ have nonvanishing perturbations Δt_l^n in a finite region so that the corresponding Dyson equation

$$G_{LL'}^{nn'}(E) = G_{LL'}^{0,nn'}(E) + \sum_{n''L''} G_{LL''}^{0,nn''} \Delta t_{l''}^{n''} G_{L''L'}^{n''n'} \tag{12}$$

can be solved by matrix inversion in real space, possibly by again taking advantage of the point group symmetry of the system.

For layered systems with a two-dimensional 'in-plane' periodicity it is advisable to use a mixed representation with the in-plane degrees of freedom considered in reciprocal space and the perpendicular-to-plane coordinates in real space. This results in a Green function $G_{LL'}^{ii'}(\boldsymbol{k}_\parallel; E)$ with layer indices i and i' which contains both the energy E and the $\boldsymbol{k}_\parallel$ vectors as parameters. The resulting Dyson equation with the corresponding ideal crystal Green function as the reference

$$G_{LL'}^{ii'}(\boldsymbol{k}_\parallel; E) = G_{LL'}^{0,ii'}(\boldsymbol{k}_\parallel; E) + \sum_{i''L''} G_{LL''}^{0,ii''}(\boldsymbol{k}_\parallel; E) \Delta t_{l''}^{i''} G_{L''L'}^{i''i'}(\boldsymbol{k}_\parallel; E) \tag{13}$$

has the structure of the equation for a linear chain with atoms i and i'. For a finite number of perturbed layers the solution can be obtained by inversion. In this way accurate calculations for surfaces can be performed by removing the atomic potentials in a few, e.g. five, layers, so that two half-infinite crystals are formed, which due to the strong vacuum barrier are practically not coupled.

This method has, however, several disadvantages. First, by relying on the ideal crystal as the reference, both halfspaces are necessarily identical, which is a serious limitation for layered systems. Second, layer relaxations are difficult to describe since reference is made to the ideal positions. Moreover, the numerical effort scales like the third power of the number N of the perturbed layers. All this is avoided by the much more elegant and efficient screened KKR scheme to be presented in section 3.

The availability of the Green function for the surface or for a layered system again allows the treatment of perturbations like an impurity or a small cluster in this system. The resulting Dyson equation is the same as for the impurity-in-bulk case (12) except that the Green function $G_{LL'}^{0,nn'}$ has to be replaced by, e.g., the surface Green function and the perturbations Δt_l^n refer to the deviations from the unperturbed surface values. In our group we have used this method in numerous calculations investigating the strongly enhanced magnetism of single adsorbate atoms and small clusters on surfaces [20–23].

2. Full potential KKR method, forces and lattice relaxations

2.1. Full potential

All-electron methods based on a spherical potential of muffin-tin type or on the atomic sphere approximation (ASA) have in general proven to be very successful and efficient for the description of the electronic structure of solids. However, systems with lower symmetry and/or open structures require a more accurate treatment going beyond the spherical approximation. This is also necessary, if forces and lattice relaxations are calculated, since for these problems the spherical approximation fails completely. We show in this section that the KKR method can be extended into an accurate and efficient full potential method, fulfilling all desired requirements for successful electronic structure calculations. We will not discuss the strongly debated l-convergence problems of the KKR method for the case of full potentials [4, 7, 19]. To a large extent we consider these as a more mathematical problem, which in practical applications does not prevent highly accurate calculations with low $l_{\max}$-cut-offs of $l_{\max} = 3$ or 4.

As we demonstrate in this section, such full potential KKR calculations have the same accuracy as the FLAPW method.

The fundamental equation (6) for the KKR–Green function is also valid in the full potential case so that the important separation between the single-potential problem and the multiple scattering problem survives fully. However the single-site eigenfunctions $R^n_L(\boldsymbol{r}; E)$ and $H^n_L(\boldsymbol{r}; E)$ are now the solutions for the general potential $v^n(\boldsymbol{r})$ no longer being spherical [19]. For instance, $R^n_{L'}(\boldsymbol{r}; E)$ is the solution of the Schrödinger equation for a spherical wave $j_{l'}(\sqrt{E}r)Y_{L'}(\boldsymbol{r})$ incident on the potential $v(\boldsymbol{r})$

$$R_{L'}(\boldsymbol{r}; E) = j_{l'}(\sqrt{E}r)Y_{L'}(\boldsymbol{r}) + \int \mathrm{d}^3r' g(\boldsymbol{r}, \boldsymbol{r}'; E)v(\boldsymbol{r}')R_{L'}(\boldsymbol{r}'; E) \tag{14}$$

where $g(\boldsymbol{r}, \boldsymbol{r}'; E)$ is the Green function for free space. Clearly, the index L' refers to the angular momentum of the incoming partial wave. Solving equation (14) in this form would require a three-dimensional integration. By expanding both the potential as well as the wave function $R_{L'}(\boldsymbol{r}; E)$ into spherical harmonics

$$v(\boldsymbol{r}) = \sum_L v_L(r)Y_L(\boldsymbol{r}) \tag{15}$$

$$R_{L'}(\boldsymbol{r}; E) = \sum_L R_{LL'}(r)Y_L(\boldsymbol{r}) \tag{16}$$

we obtain coupled radial equations for the double-indexed radial functions $R_{LL'}$

$$R_{LL'}(r; E) = \delta_{LL'}j_{l'}(\sqrt{E}r) + \int_0^S \mathrm{d}r' r'^2 g_l(r, r'; E) \sum_{L''} v_{LL''}(r)R_{L''L'}(r'; E). \tag{17}$$

Here the first index L refers to the $\boldsymbol{r}$-coordinate of the outgoing partial wave and the second one L' to the angular momentum of the incoming wave. The radial integral extends up to the range S of the potential. Moreover,

$$v_{LL'}(r) = \sum_{L''} C_{LL'L''}v_{L''}(r) \tag{18}$$

where $C_{LL'L''} = \int \mathrm{d}\Omega\, Y_L Y_{L'} Y_{L''}$ are the Gaunt coefficients.

The solution of the integral equation (17) or of the equivalent differential equation

$$\sum_{L''} \left[\left(-\frac{1}{r}\frac{\partial^2}{\partial r^2}r + \frac{l(l+1)}{r^2} - E \right) \delta_{LL''} + v_{LL''}(r) \right] R_{L''L'}(r; E) = 0 \tag{19}$$

is rather complicated [29]. In order to avoid numerical problems we have transformed equations (17) into a modified integral equation [18], where the effect of the spherical part of the potential is already included in the incident radial wave function $\overset{\circ}{R}_l(r, E)$

$$R_{LL'}(r, E) = \delta_{LL'}\overset{\circ}{R}_l(r, E) + \int_0^S \mathrm{d}r' r'^2 G_l(r, r'; E) \sum_{L''} \Delta v_{LL''}(r)R_{L''L'}(r'; E) \tag{20}$$

and where $G_l(r, r'; E)$ is the l-dependent radial Green function for the spherical component of the potential

$$G_l(r, r'; E) = \sqrt{E}\,\overset{\circ}{H}_l(r_>; E)\,\overset{\circ}{R}_l(r_<; E) \tag{21}$$

and $\Delta v_{LL'}$ the non-spherical component of the potential

$$\Delta v_{LL'}(r) = \sum_{L''\neq 0} C_{LL'L''}v_{L''}(r) \tag{22}$$

which provides the coupling between the different angular momenta. Since the non-spherical potential Δv is always rather small, we solve equation (20) by iteration, being equivalent to a Born series expansion in powers of Δv. Usually two to four iterations are sufficient for convergence. However, 10 or 20 iterations are not prohibitively expensive, so that in practical cases this iteration procedure does not present an approximation.

While for non-spherical potentials the general equation (6) for the Green function remains valid and only $R_L(\boldsymbol{r})$ and $H_L(\boldsymbol{r})$ have to be replaced by the single-site solutions for the anisotropic potential, the same is also true for the Dyson equation (9) describing multiple scattering. Only the t-matrix $t_l^n(E)$ has to be replaced by the t-matrix $t_{LL'}^n(E)$ for a general potential $v^n(\boldsymbol{r})$ being given by

$$t_{LL'}^n(E) = \int_0^S \mathrm{d}r' r'^2 j_l(\sqrt{E}r') \sum_{L''} v_{LL''}^n(r') R_{L''L'}^n(r'; E). \tag{23}$$

Since the Green functions occurring in the Dyson equation are anyhow L, L'-matrices, the numerical effort in solving the multiple scattering problem is the same for both, the spherical and non-spherical potentials. Therefore, the additional numerical effort for full potentials scales in the KKR method only linearly with the number N of non-equivalent atoms. This advantage is a direct consequence of the multiple scattering character of the KKR method, meaning that in typical calculations the full-potential method does not require a significant increase in computing time. This is particularly true for two- or three-dimensional systems, where the Dyson equation includes an additional k-loop.

In the case of a full-potential treatment the Wigner–Seitz (WS) spheres used in the atomic sphere approximation (ASA) have to be replaced by the exact WS cells, which are non-overlapping and fill the whole space completely. This is done by the use of a step function $\Theta(\boldsymbol{r})$ which is one inside the WS polyhedron and zero outside, and is used to truncate the potential outside the cell. All integrals are convoluted with $\Theta(\boldsymbol{r})$ which is expanded in spherical harmonics:

$$\Theta(\boldsymbol{r}) = \sum_L \Theta_L(r) Y_L(\boldsymbol{r}). \tag{24}$$

The expansion coefficients can be calculated for polyhedra of an arbitrary shape [30, 31]. Note that the expansion (24) converges very slowly. However, this is not a real problem for the calculations, since expanding the wave functions in spherical harmonics and restricting the angular momentum expansion to a cut-off $l_{\max}$ imposes a natural cut-off of $2l_{\max}$ for the charge density and the potential. Therefore, in the evaluation of the Coulomb integrals naturally only Θ_L-coefficients up to $4l_{\max}$ are required and this cut-off is also highly accurate for the exchange correlation terms. Thus the slow convergence of equation (24) is irrelevant. This is a direct consequence of the property of the Gaunt coefficients: $C_{LL'L''} \neq 0$ only when $|l' - l''| \leqslant l \leqslant l' + l''$.

A similar full-potential extension for the Dirac equation is also possible and a full-potential, spin-polarized, relativistic KKR method was presented in [29] together with applications for the elemental ferromagnets Fe, Co, Ni.

2.2. Full-potential results for bulk systems and surfaces

The full-potential KKR–Green function method was used for the calculation of the cohesive properties for a series of metals and semiconductors in [16]. In table 1 we compare the FP KKR results for the lattice constants and bulk moduli of seven metals, with calculations using the FLAPW method. In both cases the local density approximation has been used. As is seen, the

Table 1. Comparison of lattice constants and bulk moduli of selected metals calculated by two full-potential methods: the full-potential KKR using the LDA (FP KKR LDA) or using the generalized gradient approximation (FP KKR GGA) and the full-potential linearized augmented plane wave method (FLAPW) using the LDA (FLAPW LDA).

	Al	Fe	Ni	Cu	Rh	Pd	Ag
Lattice constants (a.u.)							
FP KKR (LDA)	7.52	5.20	6.46	6.63	7.09	7.25	7.53
FLAPW (LDA)	7.51	5.18	6.46	6.63	7.09	7.25	7.54
FP KKR (GGA)	7.64	5.34	6.63	6.84	7.22	7.43	7.80
Experiment	7.65	5.42	6.66	6.84	7.19	7.35	7.72
Bulk Modulus (Mbar)							
FP KKR (LDA)	0.82	2.43	2.54	1.88	3.18	2.28	1.39
FLAPW (LDA)	0.85	2.57	2.56	1.90	3.12	2.29	1.41
FP KKR (GGA)	0.73	1.88	2.00	1.38	2.58	1.72	0.98
Experiment	0.72	1.68	1.86	1.37	2.70	1.81	1.01

Table 2. Surface energies of the low index surfaces of Cu, Rh, and Pd. Comparison between FP-KKR and other theoretical calculations and experiment.

γ (Jm^{-2})	FPKKR	*FCLMTO* [a]		Experiment
Cu (111)	1.91	1.95	1.59[b]	1.79[e], 1.83[f]
(001)	2.15	2.17	1.71[b]	
(110)	2.31	2.24	1.85[b]	
Rh (111)	2.65	2.47	2.53[c], 2.85[d]	2.66[e], 2.70[f]
(001)	3.12	2.80	2.81[c], 3.28[d]	
(110)	3.22	2.90	2.88[c], 2.37[d]	
Pd (111)	2.01	1.92	1.64[c]	2.00[e], 2.05[f]
(001)	2.22	2.33	1.86[c]	
(110)	2.39	2.23	1.97[c]	

[a] Full charge LMTO Green function in [37].
[b] Pseudopotentials in [39].
[c] FP-LMTO in [38].
[d] Pseudopotentials in [40].
[e] Experiment in [44].
[f] Experiment in [45].

differences between the two *ab initio* methods are very small. Additionally, we present results using the generalized gradient approximation (GGA) to the exchange correlation potential. In all cases the GGA corrects the well-known LDA over-binding and is in better agreement with the experimental data. However, it is worth pointing out that the full potential is not crucial for the calculation of cohesive properties of the elemental metals. Our calculations show that accurate cohesive properties can also be obtained with spherical potentials, provided the full charge density is taken into account and all space integrals for the Coulomb and exchange-correlation energies are extended over the Wigner–Seitz polyhedra (instead of Wigner–Seitz spheres) [16]. This eliminates most of the inaccuracies of the standard ASA method.

Including the full anisotropic potential should be more decisive for systems of lower symmetry like surfaces. In table 2 we have collected the surface energies of the low-index surfaces of Cu, Rh and Pd. We compare our FP KKR results with other calculations in the literature and with other experiments. No lattice relaxation was taken into account in the FP KKR results. As we can see, the method provides surface energies in good agreement with the

experimental results and other calculations. A detailed discussion about the surface energies can be found in the study of Galanakis *et al* [41, 42]. This study shows that the orientation dependence of the surface energies of the fcc metals is well described by the 'broken-bond rule': for different orientations the surface energy scales accurately with the number of broken nearest neighbour bonds.

2.3. Forces and lattice relaxations

Accurate treatment of the full potential is crucial for the calculation of forces, since in deriving an expression for the force, the extremal properties of the total energy are used so that the force formula is no longer variationally invariant. By taking the derivative of the total energy with respect to the coordinate $\boldsymbol{R}^m$ of atom m, the force is given by

$$\boldsymbol{F}^m = -\frac{\partial E}{\partial \boldsymbol{R}^m}|_{n(\boldsymbol{r};\boldsymbol{R}^m)} - \int \mathrm{d}^3 r \, \frac{\delta E}{\delta n(\boldsymbol{r})} \frac{\partial n(\boldsymbol{r};\boldsymbol{R}^m)}{\partial \boldsymbol{R}^m}. \tag{25}$$

The first term, to be evaluated for constant density $n(\boldsymbol{r};\boldsymbol{R}^n)$, is the Hellmann–Feyman (HF) force, while the second term gives corrections due to approximations made in the solution of the Kohn–Sham equations. It vanishes in an exact treatment, since then $\frac{\delta E}{\delta n(\boldsymbol{r})} = E_F$ is a constant. Within the full-potential KKR formalism, the Kohn–Sham equations for the valence electrons are solved almost exactly, with the only approximation being the $l_{\max}$ cut-off. However, the use of the HF formula, i.e. the first term in (25), also requires a full-potential treatment of the core electrons. If an atom is shifted, the charge density of the core electrons experiences in a solid a small anisotropic distortion induced by the crystal field, which leads to an important contribution to the force on the nucleus and which unfortunately cannot be described in a spherical-core treatment. This problem can be overcome by making a spherical ansatz for the core density entering in the total-energy expression. The force is then calculated as a derivative of the total energy with respect to the nuclear position assuming that the Kohn–Sham equations are solved exactly for the valence electrons only. The resulting expression for the force $\boldsymbol{F}^m$ on the atom $\boldsymbol{R}^m$ is given by

$$\boldsymbol{F}^m = Z^m \frac{\partial V_M(\boldsymbol{r})}{\partial \boldsymbol{r}}|_{\boldsymbol{r}=\boldsymbol{R}^m} - \int \mathrm{d}^3 r n_c(|\boldsymbol{r}-\boldsymbol{R}^m|) \frac{\partial V(\boldsymbol{r})}{\partial \boldsymbol{r}} \tag{26}$$

where Z^m is the nuclear charge and $n_c(\boldsymbol{r}-\boldsymbol{R}^m)$ the core charge density of atom m. Furthermore, $V_M(\boldsymbol{r})$ is the Madelung potential and $V(\boldsymbol{r})$ the Kohn–Sham potential. While the first term is the force on the nucleus as given by the Hellmann–Feynman theorem (but without the contribution from the core electrons at atom $\boldsymbol{R}^m$), the second term represents the force on these core electrons and also includes an exchange-correlation contribution, arising from the exchange between the valence and core electrons. Thus basically (26) gives the force on the ion consisting of the nuclear charge and the core charge of atom m. We note that contrary to basis-set methods like the LMTO [33] or the FLAPW [34, 35] no finite-basis-set corrections [32] occur in the KKR formalism. Due to the vector character of the potential derivatives in equation (26), only the $l = 1$ components of the potentials $V_M(\boldsymbol{r})$ and $V(\boldsymbol{r})$ are needed for the force. Since in the present full-potential treatment the coefficients $V_L(r)$ are anyhow calculated during the self-consistency cycles, the calculation of the force does not require additional efforts. Moreover, the $l = 1$ components of the potentials are essentially determined by the $l = 1$ components of the valence charge density $n(\boldsymbol{r})$. Therefore, one obtains only contributions from the interference of wave functions differing by $\Delta l = \pm 1$, i.e. sp, pd, df, fg, ... interference terms. For these reasons we find that the convergence of the force expression (26) with respect to the maximal angular momentum $l_{\max}$ for the wave functions is unproblematic. For instance, in the cases given below, $l_{\max} = 4$ gives reliable results for transition metals, while for semiconductors

$l_{\max} = 3$ is sufficient. Additional complications in the force calculation can arise from the higher core states. The core states are calculated within muffin-tin spheres to ensure the vanishing overlap between the core electrons of neighbouring atoms. For the more extended semi-core states, the confinement within the muffin-tin sphere might lead to errors in the core energies. To overcome this problem, higher core states are treated on the same footing as valence electrons by starting the energy integration at an energy, which is below the energies of these semi-core states [25].

In contrast to the simplicity of the force calculation, the description of lattice relaxation effects is rather complicated within the KKR method. The main reason is the site-centered angular momentum expansions used in the Green function. In the case of lattice relaxations one needs an angular momentum expansion around the shifted position, i.e. around a non-lattice site. While, in principle, the host Green function can be calculated for any interstitial site by introducing a supercell with additional empty positions, this is a cumbersome procedure for the small lattice relaxations occurring for substitutional defects. In this case a transformation formalism, used e.g. in [25], is more convenient. The structural host Green function is transformed from the unshifted coordinates to new coordinates being shifted by $\boldsymbol{s}^n$

$$\tilde{G}^{nn'}_{LL'}(E) = \sum_{L''L'''} U_{LL''}(\boldsymbol{s}^n; E) G^{nn'}_{L''L'''}(E) U_{L'L'''}(\boldsymbol{s}^{n'}; E) \tag{27}$$

where

$$U_{L'L}(\boldsymbol{s}; E) = 4\pi \sum_{L''} \imath^{l'+l''-l} C_{LL'L''} j_{l''}(\sqrt{E}s) Y_{l''}(\boldsymbol{s}). \tag{28}$$

The $\tilde{G}$ is the host Green function but expanded in the shifted coordinate system. An analogous U transformation has to be made for the t-matrix. Finally we must solve the following Dyson equation for the structural Green function to obtain the new Green function for potentials or t-matrices on the shifted sites.

$$\bar{G} = \tilde{G}^0 + \tilde{G}^0[t - \tilde{t}^0]\bar{G} \tag{29}$$

where $\tilde{G}^0$ and $\tilde{t}^0$ are the host Green function and host t-matrix in the angular momentum expansion around the shifted sites (27). Thus, apart from the U-transformation, the structure of the Dyson equation is unchanged. While the U-transformation (27) is exact, if the sums over L'' and L''' are extended over infinite angular momenta, in practical calculations an $l_{\max}$-cut-off is used. As can be seen from equation (28), for small s the $U_{LL'}$-matrix couples states with $l - l' = \pm 1$. Thus a relatively high $l_{\max}$ is chosen and the error increases with increasing displacements. All the following results have been obtained with $l_{\max} = 4$, and test calculations (with larger $l_{\max}$ values) show that the resulting shifts are accurate up to 10% of the nearest neighbour distance, which is completely sufficient for substitutional defects. For interstitial defects the method of Brillouin-zone integration has to be used.

2.4. Lattice relaxations around impurities

The full-potential KKR method was used for the calculation of the ground-state configuration of several defects in metals and semiconductors, and the resulting geometries were compared with other *ab initio* calculations as well as experimental data.

As an accuracy test we have calculated the total energy and the force for several atomic configurations for a Pd substitutional impurity atom in a Cu host (figure 1). First the Green function of the infinite Cu host is calculated. The local perturbation of the Pd atom and 78 Cu atoms surrounding the defect in the fcc lattice is calculated self-consistently using the Dyson equation. The first neighbours to the impurity are relaxed radially and for each atomic

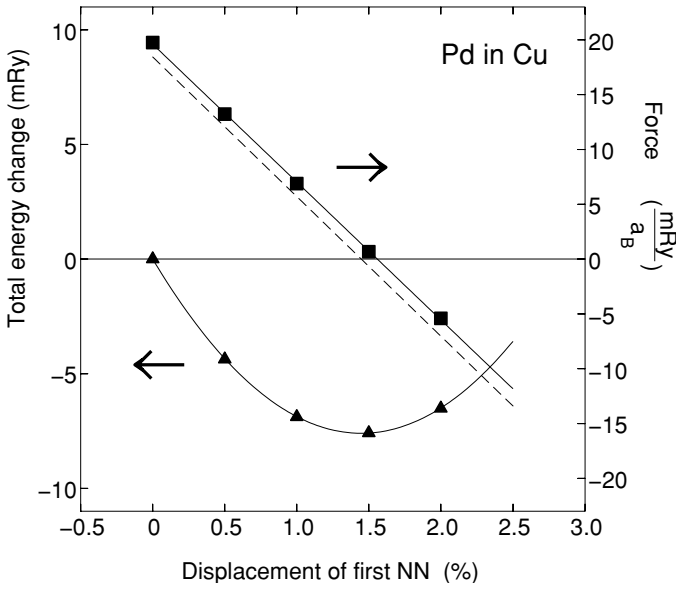

Figure 1. Total energy and radial force on a neighbouring Cu atom as a function of the nearest neighbour distance, for a Pd impurity in Cu. A linear fit for the force and a parabolic one for the energy are shown. The force is calculated both from the HF theorem and from the derivative of the fit to the total energy values (dashed line).

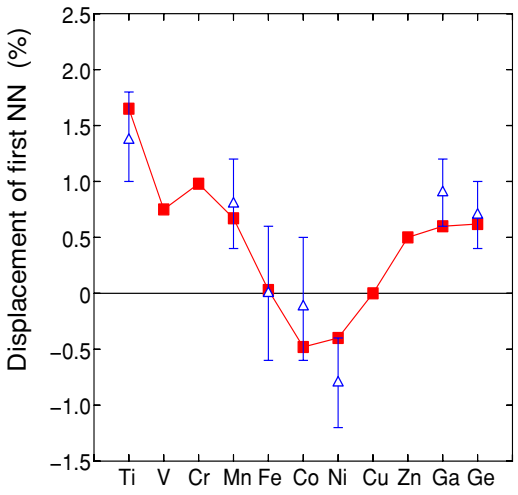

Figure 2. Calculated lattice relaxations around 3d and 4sp impurities in Cu. The displacements of the nearest neighbour Cu atoms (in percentage of the nearest-neighbour distance) are given. The triangles with error bars refer to EXAFS results.

configuration the electronic structure, the total energy and the HF force are calculated. The total energy values are interpolated by a parabolic fit, from which the force can be calculated again by differentiation (dashed line). The good agreement between the two results for the force ensures the overall consistency of the calculation and demonstrates the accuracy of the force formula. The lattice relaxation and the influence on the magnetic properties of

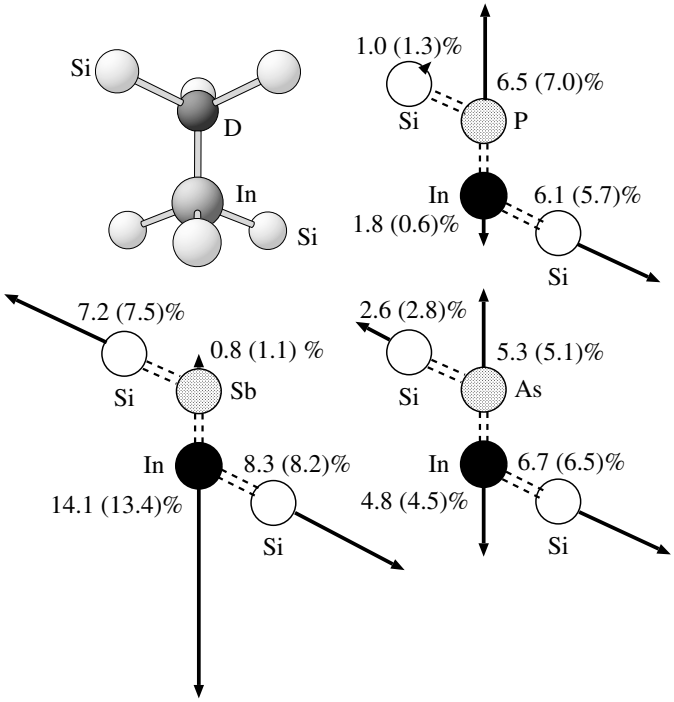

Figure 3. Ground-state configuration of In-donor complexes in Si (InSb, InP, InAs). The numbers denote the relaxations in percentage of the nearest-neighbour distance. The first number refers to KKR calculations, the second one (in brackets) to pseudopotential results.

impurities in Cu [25] and Al [26] were systematically studied. In figure 2 we present the calculated nearest neighbour shift around 3d impurities in Cu together with the experimental data from EXAFS measurements. All calculations agree well with the EXAFS data, as well as with lattice parameter measurements [25].

The accuracy of the KKR forces was also tested against pseudopotential methods [24] in calculations of the equilibrium configuration of donor–acceptor pairs in Si and Ge. These defects are electrically and magnetically inactive and experimental information about the structure is difficult to obtain. One of the few methods to investigate such defects are perturbed angular correlation (PAC) experiments which measure the electric field gradients. In figure 3 we present the calculated atomic configurations for In–P, In–Sb, In–As pairs in Si. The FP KKR results are compared with the results obtained from pseudopotential calculations. The atomic configurations obtained using both *ab initio* methods are essentially the same, but the KKR can give direct access to properties that are determined by the core electrons, like hyperfine fields or electric field gradients. The electric field gradients (EFG) of the Cd-donor pairs in Si and Ge have been measured. While calculations without lattice relaxations give the wrong trend with respect to the atomic numbers of the donor atoms, the agreement greatly improves if the relaxed configurations, as e.g. given in figure 3 for the corresponding In-pairs in Si, are considered [28]. Thus reliable calculation of the relaxations is decisive for understanding the EFG.

The effect of lattice distortions was also studied for the hyperfine fields of superheavy impurities in Fe [27], as well as on the energetics of vacancies in metals [43].

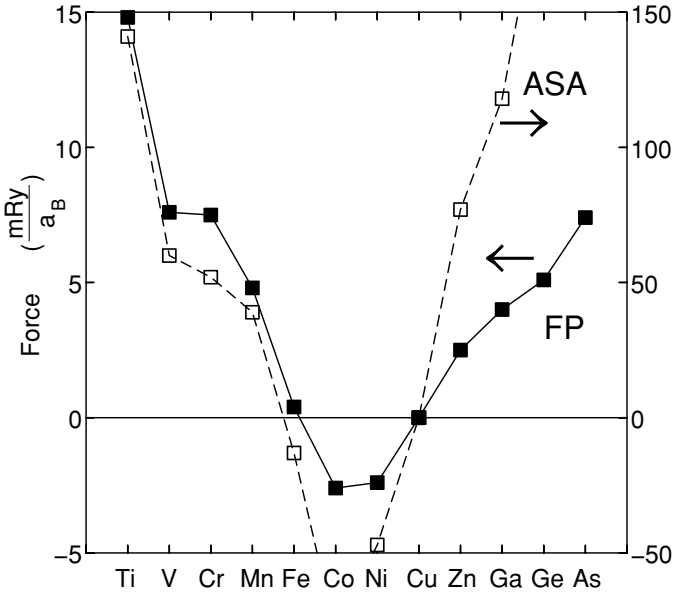

Figure 4. The *x*-component of the force exerted on the first nearest neighbours around 3d impurities in Cu. Results of full-potential calculations (full squares, left panel) and ASA-potential calculations, but including the full charge density (empty squares, right panel) are shown. Note the different scales for the ASA and FP forces.

The importance of the full potential for the force calculation is demonstrated in figure 4. The force calculated using the full potential (FP) is compared with the force obtained using a spherical potential but including the full anisotropic charge density (ASA). The force calculated using the spherical potential can reproduce the correct trend for the impurities in Cu; however, the actual values are an order of magnitude too large. Thus the calculation of atomic forces sets the limits for the validity of the spherical approximation which works quite well for most electronic properties, but fails completely in the calculation of atomic forces.

2.5. Phonon dispersions

Efficient and accurate force calculations open the possibility to study phonon dispersion relations. Frozen phonon calculations, based on supercells, are usually used to obtain the phonon frequencies for high symmetry points of the Brillouin zone. In this approach for each $\boldsymbol{k}$-value a different supercell calculation has to be performed. Here we use an alternative method in real space, which is directly related to the definition of the Born–von Karman coupling parameters and apply this to the calculation of the phonons in Al. By considering the impurity-in-bulk geometry, we shift the central Al atom by 0.5% and calculate self-consistently the forces on six neighbouring shells, which directly yields the coupling parameters between the central atom and any atom in this cluster. The effect of the finite value of the displacement is corrected by considering that only the harmonic contributions to the forces, but not the leading anharmonic corrections, change sign by inverting the direction of the shift. By Fourier transform we obtain the dynamical matrix and the phonon frequencies and eigenstates in the whole Brillouin zone. Thus this method gives for cubic crystals the whole phonon information in a single self-consistent calculation. However, a disadvantage of this approach

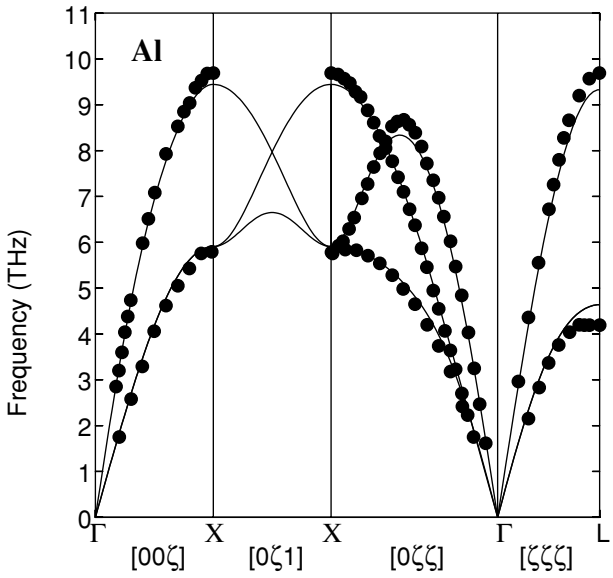

Figure 5. Calculated phonon spectrum of fcc Al together with the experiment in [35] (full dots). The calculations refer to an impurity-in-host geometry. The central Al atom is shifted by 0.5% and the forces on six shells of neighbouring atoms are calculated self-consistently, yielding force constant parameters for six nearest-neighbour shells.

is that a relatively big cluster, including many atoms, has to be used in an impurity-in-bulk configuration to account for long range elastic interactions present, for example, in semiconductors. Due to the finite shift of the central atom, anharmonic effects can also be calculated this way. In figure 5 we show the phonon dispersion of Al calculated by this procedure. As can be seen a calculation with 6 nn interactions reproduces the experimental data quite well. The same procedure was used in [27] for bcc Fe. Based on the Kanzaki model, the calculated phonon information has also been used to calculate the lattice relaxations of atoms further away from the defect [25, 27].

3. The screened (tight-binding) KKR method

In recent years much work has been addressed to improving the efficiency of first-principles density-functional calculations. A particular goal is to develop methods which show better computational complexity than the $O(N^3)$ scaling of traditional electronic-structure calculations. Here N is the system size, i.e. the number of atoms or electrons in the system. For fast calculations the traditional KKR method suffers from the fact that the structural Green function matrix elements decay very slowly in real space. Consequently, their Fourier sums converge only conditionally and require cumbersome Ewald techniques for their evaluation. In this respect a major breakthrough has been achieved by the concept of screening [46, 47], by which the KKR method can be transformed into a tight-binding form with short-range interactions between the atoms. The tight-binding formulation is very useful from the numerical point of view, since the short range of coupling allows many computational simplifications. It is important to point out here that the transformation is exact and that the resulting tight-binding KKR method works for all kind of materials, i.e. metals, semiconductors and insulators. This is in contrast to other modern $O(N)$ scaling methods, recently reviewed

by Goedecker [48], which gain their efficiency essentially from the exponential decay of the density matrix. The short-range interactions in the tight-binding KKR method are not based on the properties of the density matrix, but have a different origin as explained below.

One way to develop the tight-binding form of the KKR method has been given by Andersen *et al* [46], who showed that by generalizing the screening concept of the tight-binding LMTO method [46] to energy-dependent screening parameters [47] and by optimizing the screening parameters exponentially decreasing 'screened' structure constants can be obtained. Based on this idea Szunyogh *et al* [49] formulated a screened KKR method for surfaces and interfaces and successfully applied it in relativistic *ab initio* calculations for surfaces [50]. Unfortunately, the screened structure constants obtained according to [49] do not decrease sufficiently fast, thus limiting the accuracy.

Another method to obtain the tight-binding form of the KKR method, which is physically and mathematically more simple and transparent, is based on Green function methods and the concept of a repulsive reference system. This concept was introduced by us in collaboration with the Vienna/Budapest group [8]. For a suitably chosen reference system, for instance, consisting of an infinite array of repulsive spherical wells, the resulting structure constants decrease exponentially for energies sufficiently below the top of the well.

3.1. Theory

A simple way to understand the physics and the mathematics involved in the formulation of the tight-binding KKR method is based on the concept of an arbitrary reference system with reference potential $V^r(\boldsymbol{r})$. For two different potentials $V(\boldsymbol{r})$ and $V^r(\boldsymbol{r})$ the Green functions $G(\boldsymbol{r}, \boldsymbol{r}', E)$ and $G^r(\boldsymbol{r}, \boldsymbol{r}', E)$ are connected by an integral Dyson equation

$$G(\boldsymbol{r}, \boldsymbol{r}', E) = G^r(\boldsymbol{r}, \boldsymbol{r}', E) + \int \mathrm{d}^3 r'' G^r(\boldsymbol{r}, \boldsymbol{r}'', E)[V(\boldsymbol{r}'') - V^r(\boldsymbol{r}'')]G(\boldsymbol{r}'', \boldsymbol{r}', E) \tag{30}$$

which by the use of (1) can be verified, if the operator $-\partial_{\boldsymbol{r}}^2 + V(\boldsymbol{r}) - E$ is applied to both sides of (30). By multiple scattering theory the Dyson equation can be transformed into a system of linear equations

$$G_{LL'}^{nn'}(E) = G_{LL'}^{r,nn'}(E) + \sum_{n''} \sum_{L''} G_{LL''}^{r,nn''}(E) \sum_{L'''} \left[t_{L''L'''}^{n''}(E) - t_{L''L'''}^{r,n''}(E)\right] G_{L'''L'}^{n''n'}(E) \tag{31}$$

where space dependence only occurs in the site indices n, n', n''. The traditional reference system is empty space, where the potential and consequently the t-matrix vanish. The free-space structural Green function matrix elements $g_{LL'}^{nn'}$ are analytically known as

$$g_{LL'}^{nn'}(E) = -4\pi \mathrm{i}\sqrt{E}(1 - \delta_{nn'}) \sum_{L''} \mathrm{i}^{l+l''-l'} C_{LL'L''} h_{l''}(\sqrt{E}|\boldsymbol{R}^{nn'}|) Y_{L''}(\boldsymbol{R}^{nn'}) \tag{32}$$

with $\boldsymbol{R}^{nn'} = \boldsymbol{R}^n - \boldsymbol{R}^{n'}$ and $C_{LL'L''} = \int_{4\pi} \mathrm{d}\Omega_{\boldsymbol{r}}\, Y_L(\boldsymbol{r}) Y_{L'}(\boldsymbol{r}) Y_{L''}(\boldsymbol{r})$. Here h_l are spherical Hankel functions and Y_L spherical harmonics.

Because of this analytical formula potential-free space seems to be the easiest system and is the traditional choice for the reference system. However, it has serious disadvantages. For instance, in periodic geometries one needs Fourier sums like

$$g_{LL'}(\boldsymbol{k}, E) = \sum_{n'} \exp(\mathrm{i}\boldsymbol{k} \cdot \boldsymbol{R}^{nn'}) g_{LL'}^{nn'}(E) \tag{33}$$

which converge only conditionally and require complicated Ewald procedures [51] for their evaluation as a consequence of the slowly decaying Hankel functions in (32). This problem is connected with the fact that the traditional KKR structure constants $g_{LL'}(\boldsymbol{k}, E)$ show the

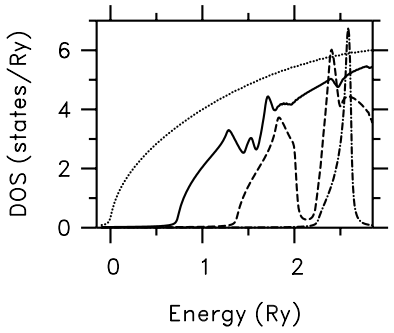

Figure 6. Density of states (DOS) for a fcc reference system. The height of the repulsive potentials is chosen as 0, 1, 2, 4 Ry and the corresponding DOS are plotted with dotted, solid, dashed and dash-dotted curves. The Brillouin-zone sampling was done with 11 726 special points in the irreducible part and smoothed by a temperature broadening with $T = 800$ K.

well-known free-electron singularities for $E = |\boldsymbol{k} + \boldsymbol{K}^h|^2$, where $\boldsymbol{k}$ denotes the wave vector and $\boldsymbol{K}^h$ a reciprocal lattice vector. Thus the numerical ineffiencies of the traditional reference system are caused by the eigenstates of potential-free space. It is much better to start from a reference system, which has no eigenstates in the energy range of the valence electrons, typically covering energies below 1 Ry. In this energy range the reference Green function would then decay exponentially. Whereas the structural Green function elements of free space are known analytically (32), the structural Green function elements $G^{r,nn'}_{LL'}(E)$ of other reference systems must be calculated numerically according to

$$G^{r,nn'}_{LL'}(E) = g^{nn'}_{LL'}(E) + \sum_{n''} \sum_{L''} g^{nn''}_{LL''}(E) \sum_{L'''} t^{r,n''}_{L''L'''}(E) G^{r,n''n'}_{L'''L'}(E). \tag{34}$$

It is easy to show [8] that the structural Green function elements $G^{nn'}_{LL'}(E)$ of the real system do not depend on the choice of the reference system. This arbitrariness of the reference system can be exploited to make the Green function elements $G^{r,nn'}_{LL'}(E)$ exponentially decaying with the distance $|\boldsymbol{R}^n - \boldsymbol{R}^{n'}|$. As a consequence exponentially small matrix elements $G^{r,nn'}_{LL'}(E)$ can be neglected in (31) and (34), which enormously simplifies the calculations as detailed below.

A particular choice for a reference system, which has no eigenstates in the energy range of the valence electrons, is given by an infinite array of repulsive, constant, finite potentials within nonoverlapping spheres around each scattering centre $\boldsymbol{R}^n$ and a zero potential in the interstitial region between the spheres. It is also possible to choose infinite height for these repulsive potentials. For not too high potentials the application of first-order perturbation theory indicates that the eigenstates should be shifted to higher energies by an amount which is given by the product of potential strength and volume filling. The calculated density of states for such an potential array at fcc lattice sites with volume filling of 74% is shown in figure 6 and confirms the shift to higher energies. Contrary to first-order perturbation theory the shift is not uniform and also shows a saturation effect. The lowest eigenstate is at 0.7 Ry for potentials of 1 Ry height, at 1.35 Ry for potentials of 2 Ry height and at 2.25 Ry for potentials of 4 Ry height, whereas the estimates from first-order perturbation theory are 0.74, 1.48 and 2.96 Ry. It was shown by Zahn [52] that by increasing the potential strength the shift saturates at about 3 Ry if a maximal angular momentum $l_{\max} = 3$ is used and at about 4 Ry for $l_{\max} = 4$ or 5.

It is clear from figure 6 that there are no eigenstates below a certain energy and that the energy range is large enough for potential heights above 2 Ry in order to cover the typical

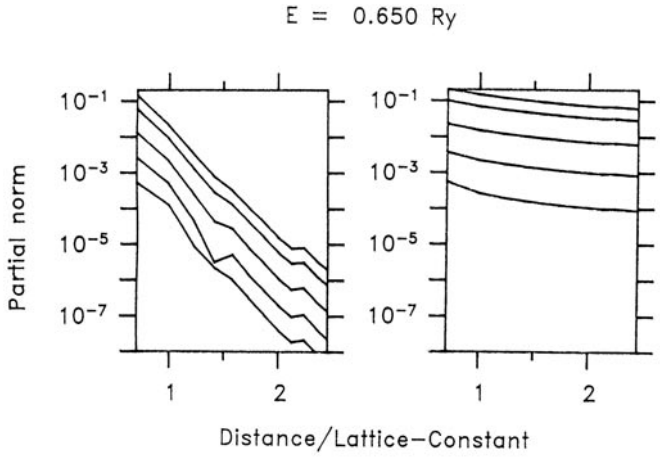

Figure 7. Screened (left panel) and unscreened (right panel) partial norms for $l = l'$ and $E = 0.65$ Ry as a function of the distance in units of the lattice constant. The results for $l = 0, 1, 2, 3, 4$ are shown from top to bottom.

valence energies occuring in ground-state calculations. The nonexistence of eigenstates means that the structural Green function matrix elements $G_{LL'}^{r,nn'}(E)$ must decay exponentially in this energy range. To visualize the decay of $G_{LL'}^{r,nn'}(E)$ as a function of $|\boldsymbol{R}^n - \boldsymbol{R}^{n'}|$, the following 'partial norm' was introduced in [8]

$$N_{ll'}(|\boldsymbol{R}^{nn'}|; E) = \frac{|E|^{(l+l')/2}}{(2l+1)!!(2l'+1)!!}\left[\sum_{mm'}\left|G_{lm,l'm'}^{r,nn'}(E)\right|^2\right]^{1/2} \tag{35}$$

with $(2l+1)!! = (2l+1)(2l-1)\ldots(3)(1)$. In figure 7 (left panel) the partial norms are plotted for $l = l'$ as a function of the distance $|\boldsymbol{R}^{nn'}|$ for the choice $E = 0.65$ Ry which is representative of the Fermi energy of Cu. They are compared with the corresponding norms of the Green function g for potential-free space in figure 7 (right panel). It is obvious from figure 7 that the partial norms for the screened structure constants $G_{LL'}^{r,nn'}(E)$ decay rapidly and essentially exponentially. Whereas the unscreened norms typically decrease by less than a factor of ten in the distance range shown in figure 7, the screened norms decrease to about 10^{-5} of their nearest-neighbour values. As a function of energy the decay remains similar as shown in [8] even up to energies less than 0.4 Ry below the lowest eigenstate of the repulsive reference system. If, of course, the energy approaches the lowest eigenstate of the reference system, then the exponential decay breaks down and the screened structure constants become strongly energy dependent.

3.2. Calculation of the tight-binding structure constants

The implementation of the tight-binding KKR method requires calculation of the tight-binding structure constants. The direct solution of (34), e.g. in periodic crystals by Fourier transformation and Brillioun-zone integration, has the same numerical complexity as the solution of (31) and can therefore not be used to speed up the calculations. Here it is important to note that the exponential decay allows restriction of the sum over n'' in (34) to a finite number of sites around $\boldsymbol{R}^{n'}$. This means that (34) can be solved independently for each site n' by taking only a finite cluster of repulsive potentials at positions $\boldsymbol{R}^{n''}$ into account.

Thus the exponential decay makes the solution of (34) suitable for parallel computing and the effort to obtain the structural Green function matrix elements $G^{r,nn'}_{LL'}(E)$ scales linearly with the number of sites n' in the system for which one wishes to calculate the electronic structure. Of course, the solution of (34) in real space with a finite number of repulsive potentials represents an approximation which one could try to minimize with particular choices of the potential wells. For nonoverlapping potentials this problem has been investigated by Zahn [52], who varied both the height of the potentials and the radii of the spheres, in which the potentials are confined. Contrary to the expectation from perturbation theory the best results are not obtained with infinite heights and touching spheres. This is a consequence of the finite $l_{\max}$-cut-off used, which does not allow description of the strong angular variation of the wave functions near the region where the hard spheres touch. Thus, either one uses touching muffin tins, but with a reduced height of for example 4 Ry, or one uses infinitely strong muffin tins, but with a reduced muffin-tin radius, e.g. reduced by 20%. In both cases the angular variations of the single-site wave functions is sufficiently smooth that an $l_{\max}$-cut-off of 3 or 4 can be used. The choice of the overlapping potentials of ASA type has been investigated in detail by Wildberger *et al* [54] and Höhler [55]. Here it turned out that ASA potentials with a cutoff at the Wigner–Seitz radius can be used and yield similarly accurate results as muffin-tin potentials. However, if the overlap becomes larger, unphysical ghost states appear in the multiple scattering contribution within the valence band range and the method totally fails. Such states also occur for ASA potentials, but only for deep negative energies, where they do not do any harm. Another idea which turned out to be not useful is to calculate the structural Green function matrix elements $G^{r,nn'}_{LL'}(E)$ very accurately by using large clusters of repulsive potentials in (34), but using only nearest neighbour couplings in (31) in order to reduce the computational effort in the solution of (31). In our experience the best procedure is the most consistent one, which uses the same coupling range for the reference Green function G^r as for the cluster of repulsive potentials.

3.3. Accuracy for density-of-states calculations

For numerical accuracy and efficiency it it interesting to know how many sites n'' must be taken into account in (34) in order to obtain accurate results. A crucial test for the tight-binding KKR method is the calculation of the electronic states for potential-free space. It is well known that the traditional KKR method gives the exact band structure and the exact density of states (DOS) for free space. The tight-binding KKR method can reproduce the exact result only up to an energy somewhat below the lowest eigenstates of the repulsive reference system and accuracy is affected by the real-space solution of (34) with a restricted sum over n''. In [53] and [54] these questions have been discussed extensively. Representative results are shown in figures 8 and 9. The density of the states shown were calculated for an empty fcc lattice with a lattice constant of 361.50 pm. The angular-momentum cut-off was $l_{\max} = 3$ and the Brillouin-zone sampling was performed by using a large number of 11 726 symmetry inequivalent points and by an artificial broadening which corresponds to a temperature of $T = 800$ K. Figure 8 shows the results as a function of energy calculated with repulsive potentials of 2, 4 and 8 Ry height and with the structure constants obtained from a finite cluster with 79 sites n''. For comparison the exact result is also shown. The curves follow the familiar square root behaviour except for a small deviation near $E = 0$ as a consequence of temperature broadening. The tight-binding KKR results agree with the exact one for lower energies. For higher energies they suddenly deviate and can also have unphysical, negative values. The energy range where the screened KKR method is applicable becomes larger for higher potentials and for larger clusters (see below) and a sudden breakdown arises when the TB parameters $G^{r,n''n'}_{L''L'}(E)$ begin to decay so slowly that solving (34) in real space makes

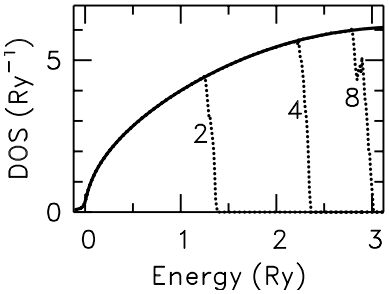

Figure 8. Density of states (DOS) for free space. Broken lines refer to screened KKR calculations, solid lines to the exact result. The numbers indicate the height (in units of Ry) of the 79 repulsive potentials used to determine the tight-binding structure constants.

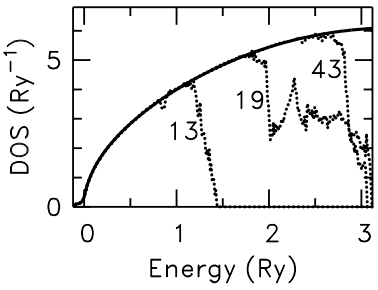

Figure 9. Density of states (DOS) for free space. Broken lines refer to screened KKR calculations, solid lines to the exact result. The numbers indicate how many repulsive potentials of height 8 Ry were used to determine the tight-binding structure constants.

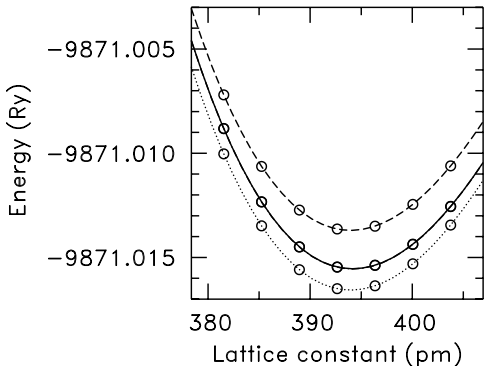

Figure 10. Total energies for Pd as a function of the lattice constant. The Brillouin-zone integrations were done with 891 symmetry inequivalent points. Dashed, dotted and solid lines refer to 13, 19 and 55 potentials of 8 Ry height which were used to determine the tight-binding structure constants. The traditional KKR result is indistinguishable from the solid line.

no sense. It is satisfying to see that accurate DOS values can be calculated almost up to energies of 3 Ry, which is clearly large enough for the calculations of occupied electronic states, but also for low-lying unoccupied ones. Figure 9 shows the results obtained by using different numbers of repulsive potentials. The energy range where the screened KKR method is applicable becomes larger if more repulsive potentials are used. For energies up to about 1 Ry the use of 13 or 19 repulsive potentials seems to be enough. As discussed below, this also remains true for self-consistent density-functional calculation with moderate accuracy.

3.4. Accuracy for total-energy calculations

Zeller [53] provides results for total energies, lattice constants and bulk moduli for the fcc metals Al, Cu and Pd as typical examples for simple, noble and transition metals. The results were obtained both by the traditional and the tight-binding KKR method with an angular-momentum cut-off $l_{\max} = 3$ in full-potential mode as described above. The calculations were nonrelativistic and the exchange-correlation potential in the parameterization of Vosko *et al* [56] was used. Representative results are shown in figure 10 and tables 3 and 4.

Table 3. Total-energy differences ΔE between traditional and screened KKR calculations with an angular-momentum cut-off $l_{\max} = 3$. The first row contains the number of repulsive potentials of height V^r which were used to determine the tight-binding structure constants. The Brillouin-zone integrations were done with 891 symmetry inequivalent points corresponding to 37 288 points in the full zone.

No of potentials		13	19	43	55	79	153	225
	V^r	ΔE						
	(Ry)	(mRy)	(mRy)	(mRy)	(μRy)	(μRy)	(μRy)	(μRy)
Al	2	6.39	0.99	0.08	−15.2	6.3	−0.27	0.05
	4	−0.19	−0.19	0.53	37.3	10.8	0.52	0.11
	8	−2.88	−0.98	1.24	57.7	26.2	1.14	0.53
Cu	2	−0.48	2.28	0.32	6.4	−13.9	−0.67	−0.03
	4	−3.38	0.62	0.28	−20.5	0.0	−0.07	0.06
	8	−3.89	0.55	0.51	−24.0	−1.0	0.11	0.34
Pd	2	−0.66	0.93	0.55	14.4	1.1	−0.18	0.06
	4	−1.84	0.59	0.63	−3.0	−1.9	−0.03	0.11
	8	−1.77	1.10	1.07	8.8	0.6	0.25	0.33

Table 4. Lattice constants a and bulk moduli B_0 for Al, Cu, and Pd determined by traditional and screened KKR calculations with an angular-momentum cut-off $l_{\max} = 3$. The potentials used to obtain the tight-binding structure constants were 8 Ry high. The Brillouin-zone integrations were done with 891 symmetry inequivalent points corresponding to 37 288 points in the full zone.

No of	Al		Cu		Pd	
potentials	a (pm)	B_0 (GPa)	a (pm)	B_0 (GPa)	a (pm)	B_0 (GPa)
13	402.22	80.69	358.52	165.41	393.97	178.33
19	401.08	80.64	358.02	170.83	393.97	179.48
43	400.96	81.21	358.18	168.91	394.02	180.22
79	400.93	81.49	358.20	169.68	394.16	178.82
Traditional	400.93	81.47	358.20	169.63	394.16	178.78

Figure 10 displays the total energy calculated for Pd as a function of the lattice constant. Whereas the results obtained with tight-binding structure constants calculated from finite clusters with 13 or 19 repulsive potentials differ by about 2 or 1 mRy from the exact results, the results obtained by using a finite cluster with 55 repulsive potentials are indistinguishable from the exact results. A detailed account of the total-energy differences is given in table 3. For structure constants determined from (34) with 153 or 225 repulsive potentials, the total energies differ less than 1 μRy from the values of standard KKR calculations. For 225 potentials of 2 or 4 Ry height the total energies even agree within 0.1 μRy. This means that total energies of the order a several thousands Ry can be obtained with a relative precision of 10^{-10}. If a moderate mRy accuracy is sufficient, nearest-neighbour couplings (13 sites) are enough to determine the structural Green function matrix elements of the repulsive reference system.

Table 4 shows for the same fcc metals also that equilibrium properties like lattice constants and bulk moduli can be calculated by the tight-binding KKR method with high accuracy. Typical errors for total energies, lattice constants and bulk moduli are 1 mRy, 0.2 pm and 1 GPa, if 19 potentials of 8 Ry height on central, nearest and next-nearest neighbour sites are used, and 5 μRy, 0.01 pm and 0.05 GPa, if 79 potentials are used.

3.5. Efficiency for large-scale calculations

The essential simplification of the tight-binding KKR method compared to the traditional KKR method arises from the exponential decay of the tight-binding structure constants. If exponentially small elements are neglected in the Green function matrix $G^{r,nn'}_{LL'}(E)$, the matrix operations to solve (31) involve sparse matrices in the tight-binding KKR method compared to dense matrices in the traditional KKR method. Whereas general sparse-matrix algorithms to solve (31) are difficult to obtain because Green function matrices are not Hermitian but general complex matrices, the situation is much more favourable for systems with two-dimensional periodicity like multilayers, surfaces, interfaces, finite slabs, or half-infinite crystals. Here two-dimensional Fourier transformation can be exploited and the resulting structural Green function matrix contains layer indices i and $i'$and depends on the two-dimensional wave vector $\boldsymbol{k}_\parallel$. Schematically, as a function of the layer indices, the structural Green function matrix $G^{r,ii'}_{LL'}(E,\boldsymbol{k}_\parallel)$ has a sparsity structure of the form

$$\begin{bmatrix} x & x & 0 & . & 0 & 0 & x \\ x & x & x & . & 0 & 0 & 0 \\ 0 & x & x & . & 0 & 0 & 0 \\ . & . & . & . & . & . & . \\ 0 & 0 & 0 & . & x & x & 0 \\ 0 & 0 & 0 & . & x & x & x \\ x & 0 & 0 & . & 0 & x & x \end{bmatrix} \tag{36}$$

where each x denotes a nonvanishing matrix block. The blocks would be submatrices with L and L' indices, if only nearest neighbouring layers couple. For longer ranged coupling one can use the principal layer technique by which several layers are combined into a principal layer such that only nearest neighbouring principal layers couple. Then again one obtains the form (36), but now the blocks are submatrices with L and L' indices and i and i' indices enumerating the layers within the principal layer. The matrix structure displayed in (36) is the appropriate one for the multilayer geometry, whereas in slab geometry the lowest left block and the highest right block vanish. For surfaces, interfaces, halfcrystals the matrix (36) has an infinite range on one or both sides. In any case the numerical complexity is greatly reduced from $O(N^3)$ to $O(N)$ for N different layers and $O(\log N)$ for N identical principal layers. The treatment of matrices like (36) is well known in tight-binding surface physics and, for instance, for the tight-binding linear-muffin-tin-orbital method [46], Wenzien *et al* [57] have presented an efficient formalism to calculate the Green function of an ideal semi-infinite crystal and the corresponding $\boldsymbol{k}_\parallel$-resolved densities of states.

In [54] the N-scaling behaviour is demonstrated for Cu slabs of varying thickness where coupling to first and second neighbouring layers is taken into account. Figure 11 shows the computing time for the solution of the Dyson equation in one self-consistency iteration as a function of the number N of layers considered. The slope of the linear curve is changed from about 4.6 s/layer for $l_{\max} = 2$ to about 13.5 s/layer for $l_{\max} = 3$ due to the corresponding increase of the matrix size from 9×9 (for $l_{\max} = 2$) to 16×16 (for $l_{\max} = 3$). The computing time refers to a (now outdated) IBM/RS 6000 3CT workstation. Most important is that the linear proportionality to N already starts at N-values smaller than 10 and that already for such thin slabs the computing time is lower than in traditional KKR calculations. Thus accurate tight-binding KKR calculations are feasible for very large systems with two-dimensional periodicity.

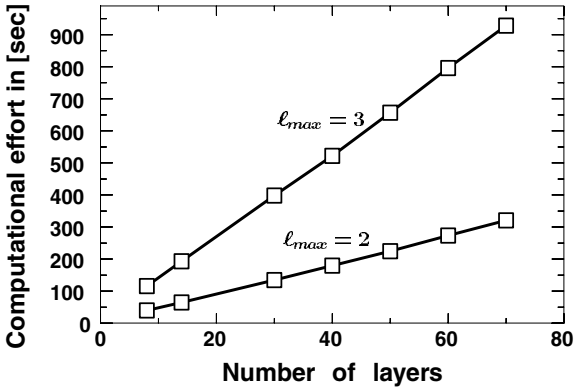

Figure 11. Computing time in seconds for solving the Dyson equation as a function of the number N of layers in the slab. One iteration with $l_{\max} = 2$, $l_{\max} = 3$, respectively, has been performed.

3.6. Recent applications

As the screened (tight-binding) KKR method greatly reduces the computational effort for layered systems due to the N-scaling, and because it greatly simplifies the calculation of the structure constants due to the discard of Ewald procedures, it has already been applied to a great variety of large and complex systems. Since the method essentially treats all electrons on an equal footing and since it is generalized in a straightforward manner to relativistic calculations, it has been particularly applied to problems in magnetism. Properties like giant magnetoresistance, magnetic anisotropy, transport through magnetic structures, interlayer exchange coupling, Bloch wall thickness [58], surface energies [41, 42], hyperfine fields of impurities at interfaces [59] and magnetic moments of monoatomic rows on vicinal surfaces [60] belong to the problems which have been investigated. The systems treated are rather complex, e.g. calculations for the giant magnetoresistance of layered systems are performed for ideal interfaces [61], for interfaces with impurities [62], for interfaces between elemental metals and alloys [66]. Calculations for the magnetic anisotropy include metals [67], systems with metallic overlayers [63] and with ordered and disordered overlayer alloys [63–65]. Transport calculations have been performed for magnetic multilayers [71] and magnetic tunnel junctions [68–70]. The largest systems treated up to now include monoatomic rows on vicinal surfaces [60] where up to 60 inequivalent atoms, i.e. 30 layers and 2 inequivalent atoms per layer, are studied and the Bloch wall thickness in bcc Fe [58], where up to 800 layers are investigated.

4. Conclusions

We have presented in this paper two recent improvements of the KKR Green function method. The first one is the extension into a full-potential scheme, which preserves the characteristic division into single scattering and multiple scattering properties of the KKR method. As we have demonstrated, the accuracy of the method is comparable to the FLAPW method, while the additional effort compared to the spherical potentials is rather modest and affects only the N-scaling single-scattering parts. The full potential method allows a straightforward calculation of the forces and the calculated relaxations around the defects agree well with experimental results.

The second recent achievement is the screened (or tight-binding) KKR method. This is basically a reformulation of multiple scattering theory in terms of exponentially decreasing

structure constants, which can be obtained by an exact screening transformation. As we have demonstrated, this screened KKR method has the same accuracy as the standard KKR method. The screened structure constants are easy to use and have no singularities. The biggest advantage of the new method is that it allows N-scaling calculations for layered systems. All these systems, a finite number of monolayers, i.e. a 'slab', a halfcrystal or two coupled halfcrystals with some monolayers in between, can be calculated with a rather modest effort, and, if the full-potential version is used, with FLAPW accuracy.

With these properties the KKR–Green function method is an excellent tool for ground-state calculations. It is particularly well suited for nanostructures like surfaces, multilayers, impurities in the bulk or on surfaces etc. It has the further advantage of all Green function methods that the availability of the Green function allows more than just ground-state calculations. For instance, one can calculate the linear response with respect to an electric or magnetic field, whether time dependent or stationary. A special application like this is quantum transport theory as described by the Kubo–Greenwood or Landauer formalism, where the availability of the Green function means a strong simplification, in particular if transport in nanostructures is considered. Another example is the electronic structure of disordered alloys as calculated by the coherent potential approximation, where the KKR-CPA has the advantage that only diagonal disorder has to be considered. Finally, we should mention in this context also the problem of excited states. For approximations of the self-energy like GW or the dynamical mean field approximation the availability of Green functions represents an excellent starting point.

References

[1] KorringaJ 1947 *Physica* **13** 392
[2] Kohn W and Rostoker N 1954 *Phys. Rev.* **94** 1111
[3] Gonis A 1992 *Green Functions for Ordered and Disordered Systems* (Amsterdam: North Holland/Elsevier)
[4] Gonis A and Butler W H 2000 *Multiple Scattering in Solids* (New York: Springer)
[5] Weinberger P 1990 *Electron Scattering Theory for Ordered and Disordered Matter* (Oxford: Clarendon)
[6] Mertig I, Mrosan E and Ziesche P 1987 *Multiple Scattering Theory for Point Defects in Metals: Electronic Properties* (Leipzig: Teubner-Verlag)
[7] Butler W H, Dederichs P H, Gonis A and Weaver R L 1992 Application of Multiple Scattering Theory to Materials Science *MRS Symposia Proceedings No 253* (Pittsburgh: Materials Research Society)
[8] Zeller R, Dederichs P H, Újfalussy B, Szunyogh L and Weinberger P 1995 *Phys. Rev.* B **52** 8807
[9] Zeller R, Deutz J and Dederichs P H 1982 *Solid State Commun.* **44** 993
[10] Wildberger K, Lang P, Zeller R and Dederichs P H 1995 *Phys. Rev.* B **52** 11 502
[11] Bohnen K P and Ying S C 1979 *Solid State Commun.* **30** 301
[12] Dupree T H 1961 *Ann. Phys. NY* **15** 63
[13] Beeby J L 1967 *Proc. R. Soc.* A **302** 113
[14] Morgan G J 1966 *Proc. Phys. Soc.* **89** 365
[15] Zeller R and Dederichs P H 1979 *Phys. Rev. Lett.* **42** 1713
[16] Asato M, Settels A, Hoshino T, Asada T, Blügel S, Zeller R and Dederichs P H 1999 *Phys. Rev.* B **60** 5202
[17] Zeller R, Lang P, Drittler B and Dederichs P H 1992 *Application of Multiple Scattering Theory to Materials Science (MRS Symposia Proceedings No 253)* ed W H Butler, P H Dederichs, A Gonis and R L Weaver (Pittsburgh: Materials Research Society)
[18] Drittler B 1991 *Dissertation* Rheinisch-Westfälische Technische Hochschule Aachen
[19] Zeller R 1987 *J. Phys. C: Solid State Phys.* **20** 2347
[20] Lang P, Stepanyuk V S, Wildberger K, Zeller R and Dederichs P H 1994 *Solid State Commun.* **92** 755
[21] Wildberger K, Stepanyuk V S, Lang P., Zeller R and Dederichs P H 1995 *Phys. Rev. Lett.* **75** 509
[22] Stepanyuk V S, Hergert W, Wildberger K, Lang P, Zeller R and Dederichs P H 1996 *Phys. Rev.* B **53** 2121
[23] Nonas B, Cabria I, Zeller R, Dederichs P H, Huhne T and Ebert H 2001 *Phys. Rev. Lett.* **86** 2146
[24] Settels A, Schroeder K, Korhonen T, Papanikolaou N, Aretz M , Zeller R and Dederichs P H 2000 *Solid State Commun.* **113** 239
[25] Papanikolaou N, Zeller R, Dederichs P H and Stefanou N 1997 *Phys. Rev.* B **55** 4157

[26] Papanikolaou N, Zeller R, Dederichs P H and Stefanou N 1997 *Comput. Mater. Sci.* **8** 131
[27] Korhonen T, Settels A, Papanikolaou N, Zeller R and Dederichs P H 2000 *Phys. Rev.* B **62** 452
[28] Settels A, Korhonen T, Papanikolaou N, Zeller R and Dederichs P H 1999 *Phys. Rev. Lett.* **83** 4369
[29] Huhne T, Zecha C, Ebert H, Dederichs P H and Zeller R 1998 *Phys. Rev.* B **58** 10 236
[30] Stefanou N, Akai H and Zeller R 1990 *Comput. Phys. Commun.* **60** 231
[31] Stefanou N and Zeller R 1991 *J. Phys.: Condens. Matter* **3** 7599
[32] Pulay P 1969 *Mol. Phys.* **17** 197
[33] Savrasov S Y and Savrasov D Y 1992 *Phys. Rev.* B **46** 12 181
[34] Yu R, Singh D and Krakauer H 1991 *Phys. Rev.* B **43** 6411
[35] Soler J M and Williams A R 1993 *Phys. Rev.* B **47** 6784
[36] Schober H R and Dederichs P H 1981 *Phonon States of Metallic Elements (Landolt-Börnstein New Series, vol 13a)* (Berlin: Springer) p 1
[37] Vitos L, Ruban A V, Skriver H L and Kollár J 1998 *Surf. Sci.* **411** 186
[38] Methfessel M, Hennig D and Scheffler M 1992 *Phys. Rev.* B **46** 4816
[39] Rodach T, Bohnen K P and Ho K M 1993 *Surf. Sci.* **286** 66
[40] Eichler A, Hafner J, Furthmüller J and Kresse G 1996 *Surf. Sci.* **346** 300
[41] Galanakis I, Bihlmayer G, Bellini V, Papanikolaou N, Zeller R, Blügel S and Dederichs P H *Europhysics Lett.* submitted (*Preprint* cond-mat/0105207)
[42] Galanakis I, Papanikolaou N and Dederichs P H to be published (*Preprint* cond-mat/0110236)
[43] Hoshino T, Papanikolaou N, Zeller R, Dederichs P H, Asato M, Asada T and Stefanou N 1999 *Comput. Mater. Sci.* **14** 56
[44] Tyson W R and Miller W A 1977 *Surf. Sci.* **62** 267
[45] Boer F R, Boom R, Mattens W C M, Miedema A R and Niessen A K 1988 *Cohesion in Metals* (Amsterdam: North-Holland)
[46] Andersen O K and Jepsen O 1984 *Phys. Rev. Lett.* **53** 2571
[47] Andersen O K, Postnikov A V and Savrasov S Yu 1992 *Application of Multiple Scattering Theory to Materials Science MRS Symposia Proceedings No 253* ed W H Butler, P H Dederichs, A Gonis and R L Weaver (Pittsburgh: Materials Research Society)
[48] Goedecker S 1999 *Rev. Mod. Phys.* **71** 1085
[49] Szunyogh L, Újfalussy B, Weinberger P and Kollar J 1994 *Phys. Rev.* B **49** 2721
[50] Szunyogh L, Újfalussy B, Weinberger P and Kollar J 1994 *J. Phys.: Condens. Matter* **6** 3301
Szunyogh L, Újfalussy B and Weinberger P 1995 *Phys. Rev.* B **51** 9552
Szunyogh L, Újfalussy B and Weinberger P 1995 *Phys. Rev.* B **51** 12 836
[51] Ham F S and Segall B 1961 *Phys. Rev.* **124** 1786
[52] Zahn P 1998 *Dissertation* Technische Universität Dresden
[53] Zeller R 1997 *Phys. Rev.* B **55** 9400
[54] Wildberger K, Zeller R and Dederichs P H 1997 *Phys. Rev.* B **55** 10 057
[55] Höhler H 2000 Private communication
[56] Vosko S H, Wilk L and Nusair M 1980 *Can. J. Phys.* **58** 1200
[57] Wenzien B, Kudrnovský J, Drchal V and Šob M 1989 *J. Phys.: Condens. Matter* **1** 9893
[58] Schwitalla J, Györffy B L and Szunyogh L 2001 *Phys. Rev.* B **63** 104 423
[59] Bellini V, Zeller R and Dederichs P H *Phys. Rev.* B **64** 144427
[60] Bellini V, Papanikolaou N, Zeller R and Dederichs P H 2001 *Phys. Rev.* B **64** 094403
[61] Zahn P, Binder J, Mertig I, Zeller R and Dederichs P H 1998 *Phys. Rev. Lett.* **80** 4309
[62] Opitz J, Zahn P, Binder J and Mertig I 2001 *Phys. Rev.* B **63** 094418
[63] Pustagowa U, Zabloudil J, Uiberacker C, Blaas C, Weinberger P, Szunyogh L and Sommers C 1999 *Phys. Rev.* B **60** 414
[64] Szunyogh L, Weinberger P and Sommers C 1999 *Phys. Rev.* B **60** 11 910
[65] Gallego S, Muñoz M C, Zabloudil J, Szunyogh L and Weinberger P 2001 *Phys. Rev.* B **63** 064428
[66] Zahn P and Mertig I 2001 *Phys. Rev.* B **63** 104412
[67] Petit L, Beiden S V, Temmerman W M, Szotek Z and Gehring G A 2001 *J. Phys.: Condens. Matter* **12** 8439
[68] Riedel I, Zahn P and Mertig I 2001 *Phys. Rev.* B **64** 195403
[69] Uiberacker C, Wang K, Heide C and Levy P M 2001 *J. Appl. Phys.* **89** 7561
[70] Freyss M, Mavropoulos Ph, Papanikolaou N, Bellini V, Zeller R and Dederichs P H Phase Transitions at press
[71] Blaas C, Weinberger P, Szunyogh L, Levy P M and Sommers C B 1999 *Phys. Rev.* B **60** 492